Desalination and Water Treatment
www.deswater.com

doi: 10.5004/dwt.2018.21867

104 (2018) 250–256
February

Photocatalytic degradation of doxycycline on ellipsoid-like $BiVO_4$ synthesized by EDTA-assisted

Changyu Lu[a,b], Jingjing Dang[a], Chentao Hou[b], Yunjie Jiang[a], Weisheng Guan[a,*]

[a]*School of Geology and Environment, Xi'an University of Science and Technology, Xi'an 710054, China, Tel. +86-29-82334561; Fax: +86-29-82334566; emails: guanweisheng@263.net (W. Guan), pzpzlxl@163.com (C. Lu), jingjing_dang@163.com (J. Dang), 61391819@qq.com (Y. Jiang)*
[b]*School of Environmental Science and Engineering, Chang'an University, 126 Yanta Road, Xi'an 710054, China, email: 512503678@qq.com*

Received 11 August 2017; Accepted 30 December 2017

ABSTRACT

An ellipsoid-like $BiVO_4$ photocatalyst was fabricated with the assistance of ethylenediaminetetraacetic acid (EDTA) in isopropanol–water mixed solvent. The as-prepared samples were characterized by Fourier transform infrared, X-ray diffractometry, scanning electron microscopy, UV–Vis, photoluminescence spectra and alternating current impedance spectroscopy. The results indicated that the morphology and size of the samples could be remarkably influenced by the addition of EDTA, and the crystal structures would remain unchanged. The morphology evolution process of $BiVO_4$ was discussed. Meanwhile, the photocatalytic activities were evaluated by the degradation of doxycycline with visible light. Due to the effective separation of photoinduced electron–hole pairs and the improvement of electron mobility, $BiVO_4$ synthesized with 1.0 g EDTA exhibited the best photocatalytic performance.

Keywords: Photocatalysis; $BiVO_4$; EDTA-assisted; Doxycycline

1. Introduction

As an important kind of tetracycline antibiotics, doxycycline (DC) is frequently detected in water bodies and sediments around the world [1,2]. The residues of it in the soil, plants and foods converge into water bodies by the biodegradation and rain scouring [3], then migrate from water to plants, animals and humans. DC could affect organisms, change microbial activities and give rise to resistance of bacteria to antibiotics [4–6]. Biodegradation and adsorption are the traditional treatments of DC. For biodegradation, DC could adhere to microbial cells to slow its growth, so the treatment effect is not satisfactory. For adsorption, the post-treatment process of adsorbent is too complex to carry out. Compared with traditional treatments, photocatalysis technology is more effective for the degradation of DC. In recent years, semiconductor-based photocatalysts have received widespread attentions in virtue of their wide applications in wastewater treatment and sustainable energy resource such as solar cells [7–9]. What's more, photocatalytic oxidation has become an effective environmental restoration technique applied to remove DC from water [10,11]. TiO_2 is the most studied and used photocatalytic material due to its superior properties, such as nontoxicity, chemical durability and oxidization resistance [12]. Nevertheless, the wide band gap (3.2 eV) is a limiting factor of TiO_2, which means merely a small ultraviolet fraction of sun light can be utilized [13]. Therefore, the visible-light-driven photocatalysts are demanded.

$BiVO_4$ is an important Ti-free and narrower band gap (2.4 eV) photocatalyst for its unique properties: ferroelasticity [14], ionic conductivity [15], photocatalytic activities for water splitting [16,17] and degradation of harmful pollutants [18–20]. Up till now, $BiVO_4$ with various morphologies have been reported, such as star-like [21], flower-like [22], spherical [23], nanosheet [24], nanorod [25], etc. For the present,

* Corresponding author.

the synthesis of $BiVO_4$ with controllable morphology and great photocatalytic activity is much desired. Recently, $BiVO_4$ with 3D architecture morphology has gradually been in a hot research. Therefore, many surfactant agents play an important role in the synthesis route. Zhu et al. [26] fabricated $BiVO_4$ hollow microspheres in the presence of ethylenediaminetetraacetic acid (EDTA) by a microwave hydrothermal method. Zhu et al. [27] used Tween-80 as a surfactant agent for the preparation of decahedral $BiVO_4$ through a microwave hydrothermal method. Lu et al. [28] prepared dumbbell-like $BiVO_4$ hierarchical nanostructures with the assistance of PVP via a simple hydrothermal route.

In this paper, ellipsoid-like $BiVO_4$ were synthesized successfully by a hydrothermal method, in which isopropanol/water mixture was solvent and EDTA was the chelating agent. The effect of EDTA on the morphology evolution was researched by adjusting the amount of it. Then, the absorption spectra, photoluminescence (PL) spectra and alternating current (AC) impedance spectroscopy of different samples were systematically investigated. Furthermore, different samples exhibited different photocatalytic degradation of DC with visible light, and the properties of synthetic materials were also dependent on the different amounts of EDTA.

2. Materials and methods

2.1. Fabrication of $BiVO_4$ microspheres

Typically, 5 mmol $Bi(NO_3)_3{\cdot}5H_2O$ was dissolved in 30 mL isopropanol, and 5 mmol NH_4VO_3 with desired amount of (0, 0.8, 1.0 and 1.2 g) EDTA was dissolved in 10 mL distilled water. The two kinds of above solution were mixed with stirring and sonicating for 30 min. Then, the mixture was poured into a 100 mL Teflon-lined stainless-steel autoclave and heated at 160°C for 16 h. Finally, the autoclave was naturally cooled to room temperature. The obtained samples were cleaned by distilled water and absolute ethanol for several times, and then dried in the vacuum drying oven at 80°C. The samples were named as $BiVO_4$-0, $BiVO_4$-0.8, $BiVO_4$-1.0 and $BiVO_4$-1.2, respectively.

2.2. Characterization of $BiVO_4$ samples

Fourier transform infrared spectroscopy (FTIR) spectrometer (PerkinElmer, Spectrum Two, USA) was applied to obtain FTIR spectra. The crystalline structures were examined using X-ray diffraction (D/max-γB) with Cu Kα radiation (λ = 41.5418 Å). The morphologies were analyzed by field emission scanning electron microscopy (SEM; Hitachi, S-4800). In the wavelength range of 200–700 nm, UV-3600 spectrophotometer (Shimadzu Corporation, Japan) was utilized to complete the absorption spectrum using $BaSO_4$ as the reference. The PL spectra were tested on F4500 (Hitachi, Japan) PL detector at the excitation wavelength of 205 nm with photomultiplier tube voltage of 500 V. The AC impedance spectroscopy was measured in a multichannel potentiostat (VMP3, Biologic, France) using a standard three-compartment cell. 0.01 M Na_2SO_4 was used as electrolyte and Pt wire and calomel electrode were used as counter electrode and reference electrode, respectively. N_2 adsorption–desorption isotherms were measured at 77 K and the Brunner–Emmet–Teller (BET) method was used to calculate the surface area and pore size by a JW-BK122F (Beijing JWGB, China).

2.3. Photocatalytic activity measurement

First of all, 50 mL of 20 mg/L DC solution was used to dissolve 20 mg of the samples. Then, the mixture placed in the photochemical reaction instrument was stirred magnetically for 30 min, which was for reaching adsorption–desorption equilibrium of DC with the catalyst. Afterwards, along with continuous magnetic stirring, the solution was completely irradiated by 300 W Xenon lamps with a cut-off filter of 420 nm to precede photocatalytic reaction. After that, the target solution was taken out and separated by centrifugation to remove the samples at different time intervals. Finally, a UV–vis spectrophotometer (Shimadzu UV2450) was used to test the adsorption UV–vis spectra and the dates are recorded.

3. Results and discussion

3.1. FTIR

FTIR spectra of the as-prepared $BiVO_4$ samples are shown in Fig. 1. The bending vibration band of Bi–O at 616 cm^{-1} and the symmetric stretching vibration band of VO_4^{3-} at 472 cm^{-1} were observed in all samples. Additionally, the asymmetric stretching vibrations of V–O at 833 cm^{-1} were also observed [29,30]. The additional band at 1,645 cm^{-1} of sample $BiVO_4$-0 was attributed to O–H bending vibrations of water which might come from KBr kept too long in the air and became damp [30]. The high sensitive FTIR spectra revealed that the product was pure [31].

3.2. XRD analysis

The structure of as-prepared $BiVO_4$ samples was evaluated by X-ray diffractometry (XRD) analysis. XRD patterns of $BiVO_4$-0, $BiVO_4$-0.8, $BiVO_4$-1.0 and $BiVO_4$-1.2 are presented in Fig. 2(a). All the characteristic peaks of the products were in accord with the standard cards JCPDS No. 14-0688 and there were no traces of other phases. It indicated that all the samples were monoclinic $BiVO_4$ [32]. Furthermore, it was

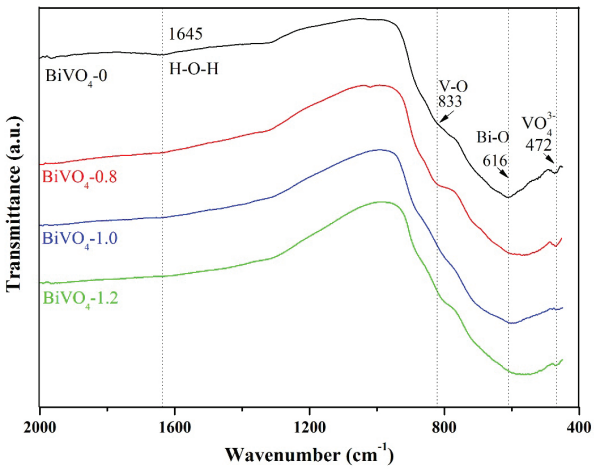

Fig. 1. FTIR spectra of different samples.

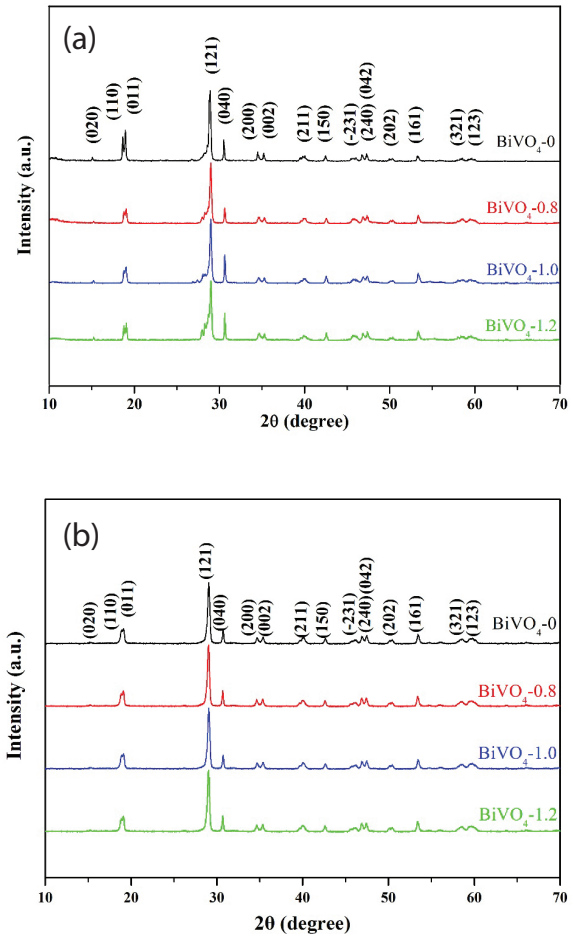

Fig. 2. XRD patterns of different $BiVO_4$ samples: (a) before irradiation and (b) after irradiation.

observed that no significant difference between the XRD patterns of different $BiVO_4$ samples, which revealed the crystalline phase of different $BiVO_4$ samples remained unchanged up with the increasing amounts of EDTA. To check the chemical stability of the materials, all the samples used methanol/acetic acid (95:5, v/v) solution eluent under ultrasonic bath for 15 min after the photocatalysis. XRD analysis for different $BiVO_4$ before and after irradiation is shown in Fig. 2(b). $BiVO_4$ spinel structure remained intact on all after irradiation catalysts and no significant peak-shift was detected which suggested as-prepared $BiVO_4$ had chemical stability.

3.3. SEM

The morphologies and microstructures of the $BiVO_4$ samples synthesized with different EDTA amounts were characterized by SEM as shown in Fig. 3. It could be obviously seen that the morphology of the $BiVO_4$ sample varied from irregular nanoparticles to ellipsoid-like with increased EDTA concentration, reflecting the increased oriented growth. First of all, the $BiVO_4$ samples in the absence of EDTA were irregular nanoparticles with the sizes ranging from 100 to 300 nm, and there was a slight agglomeration between nanoparticles (Fig. 3(a)). However, with the increasing amount of EDTA, the $BiVO_4$ samples gradually evolved into ellipsoid, which are shown in Figs. 3(b)–(d). When the amount of EDTA was 0.8 g, the $BiVO_4$ samples were irregular spheres consist of nanoparticles (Fig. 3(b)). Hence, it was possible to say that the low EDTA concentration used in the synthesis of materials was not possible to be absorbed by $BiVO_4$ primary nanoparticles in aqueous solution because the concentration employed was below the amounts of $BiVO_4$. With the addition of 1.0 g EDTA, $BiVO_4$ exhibited a uniform morphology of ellipsoid-like aggregates, of which average length and diameter were 1 μm and 400 nm, respectively (Fig. 3(c)). In addition, Fig. 3(c) also clearly reveals surface structures of the samples, it can be seen that the surfaces were rather rough and with a few of small holes. And the average size of the holes was around 100 nm. A further increase to 1.2 g, $BiVO_4$ exhibited a bigger ellipsoidal sphere, from which it was seen that the length was around 1.2 μm and the diameter was around 600 nm (Fig. 3(d)). It was found that the ellipsoid-like $BiVO_4$ was more obvious. The previous micropores disappeared in the surface which was due to concentration employed to satisfy the absorption of $BiVO_4$. It was concluded that the morphology and microstructure of $BiVO_4$ could be controlled by simply adjusting the amount of EDTA. The experimental results demonstrated that the concentration of EDTA was a vital factor in the synthesis of ellipsoid-like $BiVO_4$. The BET results included BET surface areas, pore volume and diameter are summarized in Table 1.

It is necessary to discuss the probable growth process of ellipsoid-like $BiVO_4$ in the light of the characterization results. First, the alcoholization and hydrolyzation of $Bi(NO_3)_3$ took place in isopropanol–water mixed solvent, of which the production was bismuth oxide hydroxide nitrate complex [33]. Then, Bi^{3+} was released by the dissociation of the complex. Afterwards, the released Bi^{3+} combined with VO_4^{3-} to get $BiVO_4$ primary nanoparticles quickly. Furthermore, EDTA molecules were absorbed by $BiVO_4$ primary nanoparticles gradually, and the surface energy and the growth rate of the adsorbed crystal faces all had a significant reduction. Subsequently, the $BiVO_4$ primary nanoparticles absorbed EDTA molecules and self-assembled in an oriented way to grow into ellipsoid-like samples. As for the holes, the inference of the formation mechanism was as follows. During the hydrothermal process, EDTA was unstable at high temperatures and decomposed into NO_x, CO_2, H_2O, etc., and the gas molecules congregated to form small microbubbles. Therefore, the microbubbles were the key to the holes. The exact formation mechanism needs to be further investigated. The possible formation mechanism of ellipsoid-like $BiVO_4$ is shown in Fig. 4.

3.4. UV–vis

Fig. 5 shows the UV–vis diffuse reflectance spectra of the obtained by $BiVO_4$ samples, which reflected the excellent absorption performance products had from ultraviolet to visible light area. What's more, it also revealed that the absorption edge was of approximately 520 nm. The band gap transition of the samples was the reason for the visible-light absorption, which was displayed from the steep shape of each spectrum. The band gap was determined from the equation of $\alpha h\nu = A(h\nu - E_g)^{n/2}$ [26]. In terms of $BiVO_4$, it was a direct

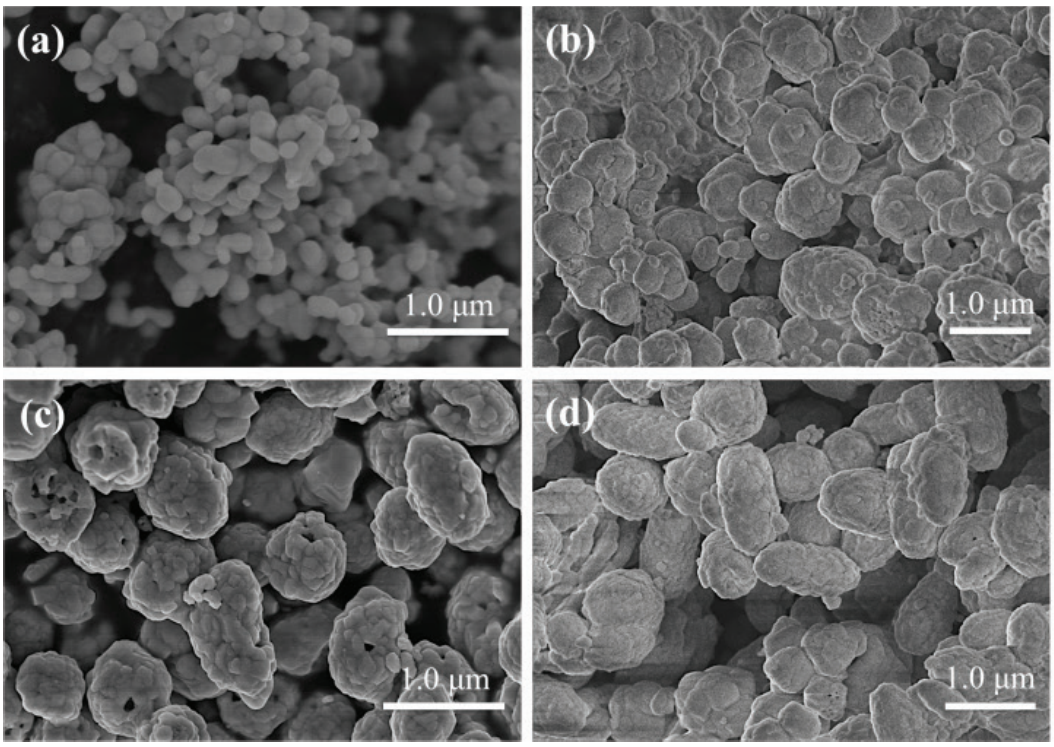

Fig. 3. SEM images of different samples: (a) $BiVO_4$-0; (b) $BiVO_4$-0.8; (c) $BiVO_4$-1.0; and (d) $BiVO_4$-1.2.

Table 1
BET surface area, pore volume, pore volume of different $BiVO_4$ samples

Sample	BET surface area ($m^2\ g^{-1}$)	Pore volume ($cm^3\ g^{-1}$)	Pore diameter (nm)
$BiVO_4$-0	0.646	–	–
$BiVO_4$-0.8	1.88	0.0029	14.3
$BiVO_4$-1.0	2.07	0.0034	16.6
$BiVO_4$-1.2	1.95	0.0032	16.2

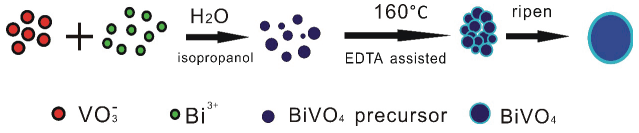

Fig. 4. Possible formation mechanism of ellipsoid-like $BiVO_4$.

band gap material, so that the value of n is 1 [34]. The band gaps of samples $BiVO_4$-0, $BiVO_4$-0.8, $BiVO_4$-1.0 and $BiVO_4$-1.2 were reckoned to be 2.42, 2.38, 2.33 and 2.40 eV, respectively. The band gap of sample $BiVO_4$-1.0 was relatively narrow compared with other samples which might be attributed to changes of morphologies, microstructures, crystalline phase and crystal structure which were affected by concentration of EDTA.

3.5. PL characteristics

Fig. 6 shows the PL spectra of samples $BiVO_4$-0 and $BiVO_4$-1.0. The PL emission maximum of $BiVO_4$-0 and $BiVO_4$-1.0 were both around 536 nm, which corresponded to the green light region. It is obvious that the PL emission intensity of $BiVO_4$-1.0 was lower than the $BiVO_4$-0. Normally, PL emission intensity of a semiconductor is proportional to the occasion of the recombination of photoinduced electron–hole pairs. It suggests that the $BiVO_4$-1.0 sample reduced the electron–hole recombination probability which facilitated the migration of electrons more effectively than $BiVO_4$-0 sample did.

3.6. AC impedance

AC impedance spectroscopy analysis is important electrochemical evidence to verify the improvement of photocatalytic performance. Fig. 7 shows Nyquist plots of samples $BiVO_4$-0 and $BiVO_4$-1.0. The semicircle of $BiVO_4$-1.0 is smaller than that of $BiVO_4$-0, which reveals a decrease in the solid-state interface layer resistance and the charge-transfer resistance on the surface [35]. It means the conductivity of $BiVO_4$-1.0 was improved which increased electron mobility. It was concluded that the enhancement of photocatalytic activity of $BiVO_4$-1.0 was due to the improvement of the electron mobility of $BiVO_4$ prepared with EDTA.

3.7. Photocatalytic performance

To further examine the application of as-prepared $BiVO_4$ samples in the removal of water contaminants, the aqueous solution of DC was taken as an example. Fig. 8 includes the photocatalytic degradation of DC under visible light illumination. Among four samples, the sample $BiVO_4$-1.0 exhibited the highest photocatalytic activity, and 88.15% of DC was degraded with irradiation for 120 min. While

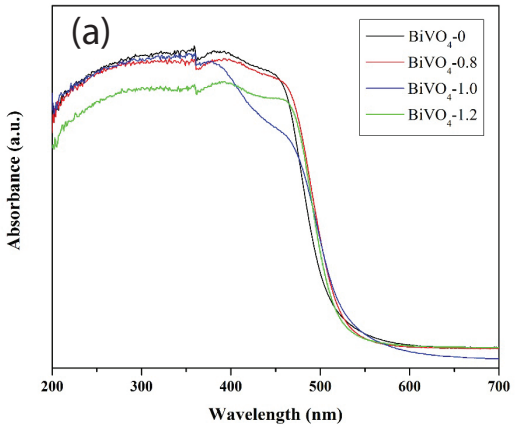

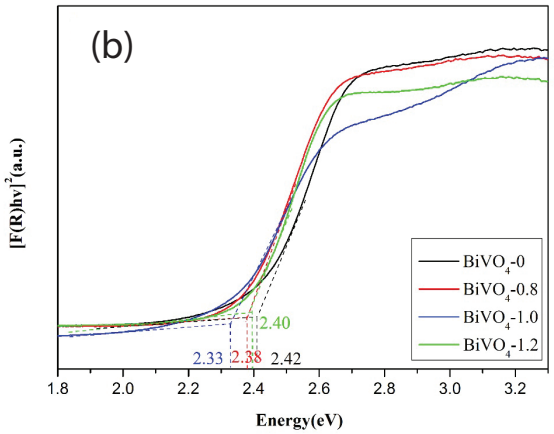

Fig. 5. UV–vis diffuse reflectance spectra of different $BiVO_4$ samples.

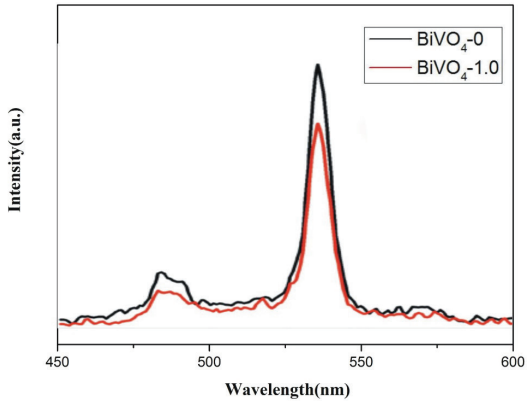

Fig. 6. PL spectra of $BiVO_4$-0 and $BiVO_4$-1.0 samples.

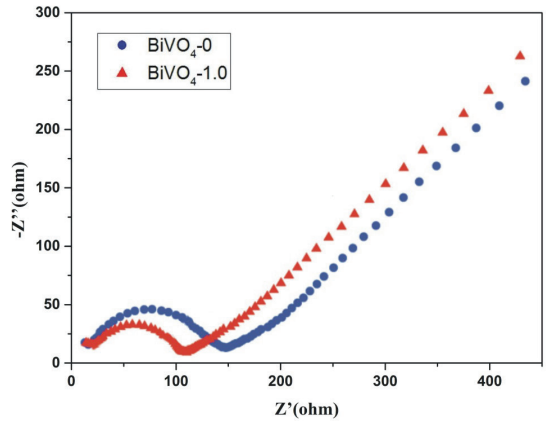

Fig. 7. Nyquist plots of $BiVO_4$-0 and $BiVO_4$-1.0 samples.

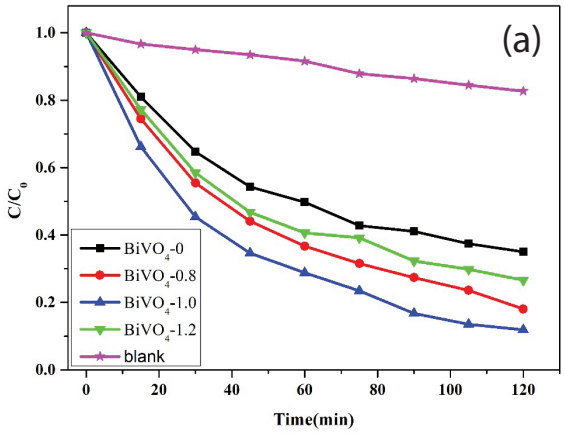

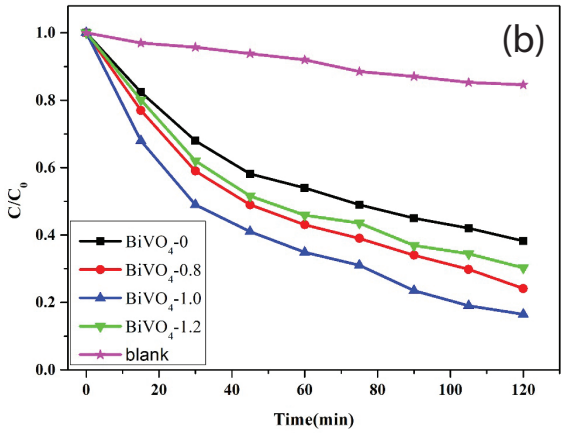

Fig. 8. The photocatalytic degradation (a) and TOC removal (b) of DC on different $BiVO_4$ samples.

the degradation of DC in the presence of blank, $BiVO_4$-0, $BiVO_4$-0.8 and $BiVO_4$-1.2 was 17.28%, 65.02%, 81.97% and 73.39%, respectively. The degradation rate (DR) of $BiVO_4$-0.8 was about 20% higher than that of $BiVO_4$-0, indicating ellipsoid-like $BiVO_4$ can greatly enhance the photocatalytic activity. The performance of ellipsoid-like $BiVO_4$ was higher than oxidative Fenton process [36] and other oxidation processes results [37,38]. However, our materials required longer reaction times to achieve equilibrium compared with catalytic Fenton system. Some reasons were proposed to account for the high photocatalytic activity of ellipsoid-like $BiVO_4$. First, as PL characteristics results, ellipsoid-like $BiVO_4$ reduced the electron–hole recombination probability and facilitated the migration of electrons more effectively,

which resulted in the higher photocatalysis capability. Second, the improvement of conductivity of ellipsoid-like $BiVO_4$ increased electron mobility. It was concluded that the enhancement of photocatalytic activity was due to the improvement of the electron mobility of ellipsoid-like $BiVO_4$ prepared with EDTA. Third, as previous results, the band gap energy of ellipsoid-like $BiVO_4$ narrowed from 2.42 to 2.33 eV, which enhanced the oxidation–reduction ability of photogenerated carriers and the photocatalytic degradation of DC.

Total organic carbon (TOC) analysis is an effective method which can be used to further demonstrate mineralization of organic pollutants, especially the properties of the photocatalysts. Fig. 8(b) shows the degradation of the organic carbon contents with different samples, the removal rates of TOC of blank, $BiVO_4$-0, $BiVO_4$-0.8, $BiVO_4$-1.0 and $BiVO_4$-1.2 samples were 15.42%, 61.77%, 75.87%, 83.54% and 69.72%, respectively. TOC contents of different samples decreased in the same order as that of the photocatalytic degradation curves (Fig. 8(a)) could also be found out from Fig. 8(b). However, the removal rates of TOC were lower than that of the DR. This result was reasonable due to the degradation data were detected after centrifugation. TOC removal and the degradation curves with similar trends indicated that photodegradation experiments had successfully eliminated the effect of physical adsorption and the photocatalytic activities of different photocatalysts were correctly evaluated. Moreover, wide environmental applications, such as the mineralization, would be implemented by $BiVO_4$, since the reduced TOC contents suggested.

4. Conclusions

In summary, a facile EDTA-assisted solvothermal method had been conducted to synthesize ellipsoid-like $BiVO_4$. The morphology and structure of different $BiVO_4$ samples were recognized by FTIR, XRD and SEM. The porous samples prepared with 1.0 g EDTA exhibited the best morphology and photocatalytic degradation of DC. In addition, several analyses such as the UV–vis diffuse reflectance spectra, PL spectra and AC impedance spectroscopy were conducted to explain improvement of photocatalytic activity which was due to the effective separation of photoinduced electron–hole pairs and the improvement of electron mobility.

Acknowledgments

This study was supported by the PhD Start-up Fund of Xi'an University of Science and Technology (No. 6310117055) and the Fundamental Research Funds for the Central Universities (No. 310829161016 and 310829161004).

References

[1] Q. Bu, B. Wang, J. Huang, S. Deng, G. Yu, Pharmaceuticals and personal care products in the aquatic environment in China: a review, J. Hazard. Mater., 262 (2013) 189–211.
[2] M.B. Ahamed, J.L. Zhou, H.H. Ngo, W. Guo, Adsorptive removal of antibiotics from water and wastewater: progress and challenges, Sci. Total. Environ., 532 (2015) 112–126.
[3] A.K. Sarmah, M.T. Meyer, A.B.A. Boxall, A global perspective on the use, sales, exposure pathways, occurrence, fate and effects of veterinary antibiotics (VAs) in the environment, Chemosphere, 65 (2006) 725–759.
[4] F. Liu, G. Ying, R. Tao, J. Zhao, J. Yang, L. Zhao, Effects of six selected antibiotics on plant growth and soil microbial and enzymatic activities, Environ. Pollut., 157 (2009) 1636–1642.
[5] J.C. Underwood, R.W. Harvey, D.W. Metge, D.A. Repert, L.K. Baumgartner, R.L. Smith, Effects of the antimicrobial sulfamethoxazole on groundwater bacterial enrichment, Environ. Sci. Technol., 45 (2011) 3096–3101.
[6] H. Su, G. Ying, R. Tao, R. Zhang, J. Zhao, Y. Liu, Class 1 and 2 integrons, *sul* resistance genes and antibiotic resistance in *Escherichia coli* isolated from Dongjiang River, South China, Environ. Pollut., 169 (2012) 42–49.
[7] R.M. Mohamed, I.A. Mkhalid, M. Abdel Salam, M.A. Barakat, Zeolite Y from rice husk ash encapsulated with Ag-TiO_2: characterization and applications for photocatalytic degradation catalysts, Desal. Wat. Treat., 51 (2013) 7562–7569.
[8] C.L. Yu, W.Q. Zhou, L.H. Zhu, G. Li, K. Yang, R.C. Jin, Integrating plasmonic Au nanorods with dendritic like α-Bi_2O_3/$Bi_2O_2CO_3$ heterostructures for superior visible-light-driven photocatalysis, Appl. Catal., B, 184 (2016) 1–11.
[9] C.L. Yu, Z. Wu, R.Y. Liu, D.D. Dionysiou, K. Yang, C.Y. Wang, H. Liu, Novel fluorinated Bi_2MoO_6 nanocrystals for efficient photocatalytic removal of water organic pollutants under different light source illumination, Appl. Catal., B, 209 (2017) 1–11.
[10] A.L. Giraldo, G.A. Penuela, R.A. Torres-Palma, N.J. Pino, R.A. Palominos, H.D. Mansilla, Degradation of the antibiotic oxolinic acid by photocatalysis with TiO_2 in suspension, Water Res., 44 (2010) 5158–5167.
[11] A. Chatzitakis, C. Berberidou, I. Paspaltsis, G. Kyriakou, T. Sklaviadis, I. Poulios, Photocatalytic degradation and drug activity reduction of chloramphenicol, Water Res., 42 (2008) 386–394.
[12] C.L.Yu, W.Q. Zhou, H. Liu, Y. Liu, D.D. Dionysiou, Design and fabrication of microsphere photocatalysts for environmental purification and energy conversion, Chem. Eng. J., 287 (2016) 117–129.
[13] N. Boujelben, F. Bouhamed, Z. Elouear, J. Bouzid, M. Feki, Removal of phosphorus ions from aqueous solutions using manganese-oxide-coated sand and brick, Desal. Wat. Treat., 52 (2014) 2282–2292.
[14] A.R. Lim, K.H. Lee, S.H. Choh, Domain wall of ferroelastic $BiVO_4$ studied by transmission electron microscopy, Solid State Commun., 83 (1992) 185–186.
[15] K. Hirota, G. Komatsu, M. Yamashita, H. Takemura, O. Yamaguchi, Formation, characterization and sintering of alkoxy-derived bismuth vanadate, Mater. Res. Bull., 27 (1992) 823–830.
[16] D. Ke, T. Peng, L. Ma, P. Cai, Photocatalytic water splitting for O_2 production under visible-light irradiation on $BiVO_4$ nanoparticles in different sacrificial reagent solutions, Appl. Catal., A, 350 (2008) 111–117.
[17] S.M. Thalluri, C.M. Suarez, S. Hernandez, S. Bensaid, G. Saracco, N. Russo, Elucidation of important parameters of $BiVO_4$ responsible for photo-catalytic O_2 evolution and insights about the rate of the catalytic process, Chem. Eng. J., 245 (2014) 124–132.
[18] Y. Zhou, W. Li, W. Wan, R. Zhang, Y. Lin, W/Mo co-doped $BiVO_4$ for photocatalytic treatment of polymer-containing wastewater in oilfield, Superlattices Microstruct., 82 (2015) 67–74.
[19] W. Ma, Z. Li, W. Liu, Hydrothermal preparation of $BiVO_4$ photocatalyst with perforated hollow morphology and its performance on methylene blue degradation, Ceram. Int., 41 (2015) 4340–4347.
[20] S.S. Xue, H.B. He, Z. Wu, C.L. Yu, Q.Z. Fan, G.M. Peng, K. Yang, An interesting Eu, F-codoped $BiVO_4$ microsphere with enhanced photocatalytic performance, J. Alloys Compd., 694 (2017) 989–997.
[21] Y. Lu, H. Shang, F. Shi, C. Chao, X. Zhang, B. Zhang, Preparation and efficient visible light-induced photocatalytic activity of m-$BiVO_4$ with different morphologies, J. Phys. Chem. Solids, 85 (2015) 44–50.
[22] W. Yin, W. Wang, M. Shang, L. Zhang, J. Ren, Preparation of monoclinic scheelite $BiVO_4$ photocatalyst by an

ultrasound-assisted solvent substitution method, Chem. Lett., 38 (2009) 422–423.
[23] U.M. García-Pérez, S. Sepúlveda-Guzmán, A. Martínez-de la Cruz, J. Peral, Selective synthesis of monoclinic bismuth vanadate powders by surfactant-assisted co-precipitation method: study of their electrochemical and photocatalytic properties, Int. J. Electrochem. Sci., 7 (2012) 9622–9632.
[24] Q. Yu, Z. Tang, Y. Xu, Synthesis of $BiVO_4$ nanosheets-graphene composites toward improved visible light photoactivity, J. Nat. Gas. Chem., 23 (2014) 564–574.
[25] X. Wang, G. Li, J. Ding, H. Peng, K. Chen, Facile synthesis and photocatalytic activity of monoclinic $BiVO_4$ micro/nanostructures with controllable morphologies, Mater. Res. Bull., 47 (2012) 3814–3818.
[26] Z. Zhu, J. Du, J. Li, Y. Zhang, D. Liu, An EDTA-assisted hydrothermal synthesis of $BiVO_4$ hollow microspheres and their evolution into nanocages, Ceram. Int., 38 (2012) 4827–4834.
[27] Z. Zhu, L. Zhang, J. Li, J. Du, Y. Zhang, J. Zhou, Synthesis and photocatalytic behavior of $BiVO_4$ with decahedral structure, Ceram. Int., 39 (2013) 7461–7465.
[28] Y. Lu, Y. Luo, D. Kong, D. Zhang, Y. Jia, X. Zhang, Large-scale controllable synthesis of dumbbell-like $BiVO_4$ photocatalysts with enhanced visible-light photocatalytic activity, J. Solid State Chem., 186 (2012) 255–260.
[29] U.M. García-Pérez, S. Sepúlveda-Guzmán, A. Martínez-de la Cruz, Nanostructured $BiVO_4$ photocatalysts synthesized via a polymer-assisted coprecipitation method and their photocatalytic properties under visible-light irradiation, Solid State Sci., 14 (2012) 293–298.
[30] U.M. García Pérez, S. Sepúlveda-Guzmán, A. Martínez-de la Cruz, U. Ortiz Méndez, Photocatalytic activity of $BiVO_4$ nanospheres obtained by solution combustion synthesis using sodium carboxymethylcellulose, J. Mol. Catal. A: Chem., 335 (2011) 169–175.
[31] S. Dong, C. Yu, Y. Li, Y. Li, J. Sun, X. Geng, Controlled synthesis of T-shaped $BiVO_4$ and enhanced visible light responsive photocatalytic activity, J. Solid State Chem., 211 (2014) 176–183.
[32] U.M. García Pérez, A. Martínez-de la Cruz, S. Sepúlveda-Guzmán, J. Peral, Low-temperature synthesis of $BiVO_4$ powders by pluronic-assisted hydrothermal method: effect of the surfactant and temperature on the morphology and structural control, Ceram. Int., 40 (2014) 4631–4638.
[33] L. Ren, L. Jin, J. Wang, F. Yang, M. Qiu, Y. Yu, Template-free synthesis of $BiVO_4$ nanostructures: I. Nanotubes with hexagonal cross sections by oriented attachment and their photocatalytic property for water splitting under visible light, Nanotechnology, 20 (2009) 115603–115611.
[34] L. Zhou, W. Wang, S. Liu, L. Zhang, H. Xu, W. Zhu, A sonochemical route to visible-light-driven high-activity $BiVO_4$ photocatalyst, J. Mol. Catal. A: Chem., 252 (2006) 120–124.
[35] H. Jiang, X. Meng, H. Dai, J. Deng, Y. Liu, L. Zhang, High-performance porous spherical or octapod-like single-crystalline $BiVO_4$ photocatalysts for the removal of phenol and methylene blue under visible-light illumination, J. Hazard. Mater., 217–218 (2012) 92–99.
[36] A.A. Borghi, M.F. Silva, S.A. Arni, A. Converti, M.S.A. Palma, Doxycycline degradation by the oxidative Fenton process, J. Chem., 2015 (2015) 1–9.
[37] J. Rivas, A. Encinas, F. Beltran, N. Graham, Application of advanced oxidation processes to doxycycline and norfloxacin removal from water, J. Environ. Sci. Health, Part A, 46 (2011) 944–951.
[38] S.M. Sunaric, S.S. Mitic, G.Z. Miletic, A.N. Pavlovic, D. Naskovicdjokic, Determination of doxycycline in pharmaceuticals based on its degradation by Cu(II)/H_2O_2 reagent in aqueous solution, J. Anal. Chem., 64 (2009) 231–237.